Engineering Structures 279 (2023) 115590

Contents lists available at ScienceDirect

Engineering Structures

journal homepage: www.elsevier.com/locate/engstruct

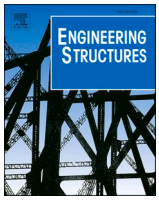

Simplified nonlinear modeling for estimating the seismic response of buildings

Jui-Liang Lin *, Ming-Chieh Chuang

National Center for Research on Earthquake Engineering, 200, Section 3, Xinhai Rd., Taipei 106, Taiwan, ROC

ARTICLE INFO

Keywords:
Nonlinear modeling
Numerical model
Seismic analysis
Generalized building model
Seismic response

ABSTRACT

Simplified nonlinear modeling for estimating the seismic response of buildings has the advantages of providing structural perception and computational efficiency. Therefore, such modeling is useful for preliminary structural design and seismic simulation of large numbers of buildings. The generalized building model (GBM), which consists of a pure shear stick, a pure flexural stick, and *N* lumped masses, has been satisfactorily used for elastic seismic analyses of *N*-story buildings in previous research. The present study develops the inelastic properties of the sticks of all stories in the GBM so that the enhanced GBM can be used for nonlinear response history analysis of buildings. The effectiveness of the enhanced GBM is verified by comparing the seismic responses of a three-story reinforced concrete building and a nine-story steel building estimated using the GBM with those obtained from corresponding finite element models.

1. Introduction

Simplified seismic analyses of buildings are generally performed using either simplified analysis methods or simplified numerical modeling. The advantage of using simplified analysis methods or simplified numerical modeling lies in the improved efficiency of its seismic evaluation, which is of course a trade-off against the accuracy of the analysis results. With regard to simplified analysis methods, using a pushover analysis method instead of nonlinear response history analysis (NRHA) appears to be one of the most popular approaches in engineering practice [1]. With regard to simplified numerical modeling, using modal systems [2–4] or stick models [5–11] instead of complete finite element models (FEMs) of building structures seems to be a common approach.

The limitations of the applicability of nonlinear static analyses (*i.e.*, pushover analyses) have been extensively investigated by comparison with nonlinear dynamic analyses. Inel et al. [12] concluded that pushover analyses can underestimate the peak inter-story drift ratio of mid-rise buildings. Additionally, pushover analyses appear to incorrectly reflect NRHA when the seismic intensity exceeds a moderate level. Aschheim et al. [13] pointed out that the accuracy of nonlinear static analyses is poor for response quantities that are significantly affected by the vibration of multiple degrees of freedom. Moreover, they proposed a design-oriented approach, referred to as the "scaled nonlinear dynamic procedure", which can be used in performance-based design. Oncu *et al* [14]. investigated the seismic responses of reinforced concrete buildings through pushover and incremental dynamic analysis methods and found strong correlations between the analysis results obtained from dynamic analysis envelopes and the static pushover curves.

Using simplified numerical modeling is advantageous for identifying critical structural parameters by which designers can efficiently grasp structural characteristics. Therefore, simplified numerical modeling is particularly suitable for preliminary design and parametric studies of building structures. Moreover, using simplified numerical modeling also makes it feasible to rapidly evaluate the seismic risk of populated cities that contain large numbers of buildings. The exploration and application of simplified numerical modeling to earthquake engineering have been comprehensively carried out. For instance, equivalent frame models were developed as a substitute for FEMs of unreinforced masonry buildings because of both the high computational cost and high analytical skill required for their nonlinear analysis [15,16]. Rodrigues et al. [17] proposed an equivalent bi-diagonal compression strut model for the simulation of the behavior of masonry infill walls. Simplified modeling techniques were also developed for simulating the soil-structure interaction (SSI) effect [8] because of the large number of degrees of freedom involved in SSI simulation and the very large computational costs. The abovementioned research is evidence that simplified numerical modeling is in great demand for dealing with the

* Corresponding author.
E-mail addresses: jllin@narlabs.org.tw (J.-L. Lin), mcchuang@narlabs.org.tw (M.-C. Chuang).

https://doi.org/10.1016/j.engstruct.2023.115590
Received 20 August 2022; Received in revised form 2 January 2023; Accepted 3 January 2023
Available online 17 January 2023

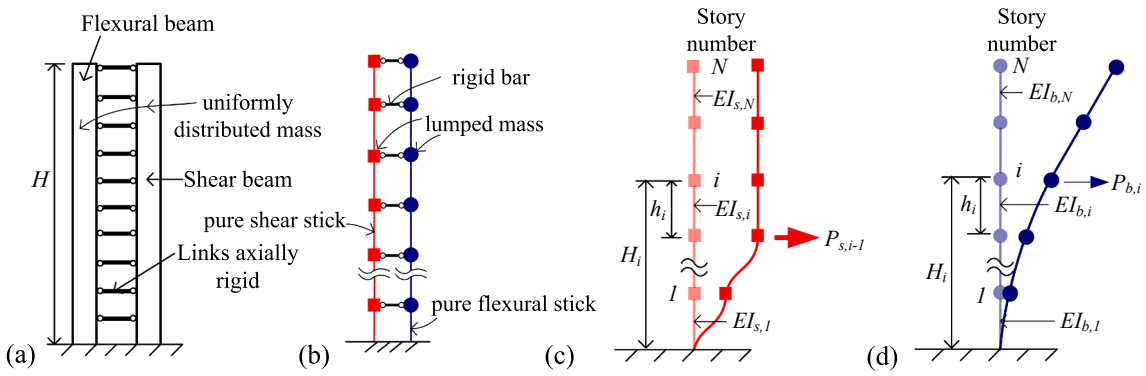

Fig. 1. (a) Continuous beam model; (b) GBM; (c) lateral deformation of a pure shear stick subjected to a concentrated lateral load, $P_{s,i\text{-}1}$, at the $(i\text{-}1)^{\text{th}}$ story; and (d) lateral deformation of a pure flexural stick subjected to a concentrated lateral load, $P_{b,i}$, at the i^{th} story.

various issues involved in earthquake engineering.

Based on the way of constructing inelastic single-degree-of-freedom (SDOF) modal systems [2], Lin and Tsai [3,4] proposed inelastic two-DOF and three-DOF modal systems for the seismic assessment of one-way and two-way asymmetric-plan buildings, respectively. These multi-DOF modal systems reveal the translational and rotational modal properties of asymmetric-plan buildings that are concealed by their counterpart SDOF modal systems. These multi-DOF modal systems are also capable of reflecting the non-proportionality that exists between the translational and rotational modal behavior of inelastic asymmetric-plan buildings [3,4]. Nakashima et al. [5] developed the generic frame model (*i.e.*, the so-called "fish-bone model") for the simulation of the earthquake response of steel moment frames by assuming all joint rotations at a floor level to be identical. Khaloo and Khosravi [6] further improved the generic frame model by modifying this assumption of equal joint rotations and incorporating flexural deformation.

Recently, Jamšek and Dolšek [19] proposed an improved fish-bone model to approximately account for the effect of the redistribution of demands between structural elements. This model substantially improved the quality of the simulation of buildings without satisfying the strong column-weak beam concept. d'Aragona et al. [20] introduced a simplified model for estimating the seismic responses of low-rise symmetric infilled moment resisting frames. The simplified model consisted of lumped masses connected through nonlinear shear links. The properties of the shear links were calibrated using a genetic algorithm procedure that utilized the results of the cyclic pushover analyses of the corresponding complete FEM. For simulating translation-rotation coupled responses, a three-dimensional (3D) reduced-order model was developed specifically for low-rise asymmetric-plan frame buildings [21]. Blasone et al. [22] also proposed a simplified 3D model for moment resisting frame buildings, in which each story has three degrees of freedom, two translational and one rotational around the vertical axis. This proposed modeling approach is capable of reflecting the effects of plan asymmetry as well as vertical irregularity. Lachanas and Vamvatsikos [23] addressed the issue of model type effects on the estimated seismic responses of a 20-story steel moment resisting frame. Based on observations of the targeted building, they concluded that the uncertainty stemming from 3D versus 2D or distributed versus lumped plasticity models is lower than the governing record-to-record variability.

The simplified models mentioned in the above paragraph focused on low-rise buildings or moment resisting frames. In order to simulate the complex behavior of elastic tall wall-frame buildings, the continuous beam model (Fig. 1a) was proposed in the 1960 s [7,8]. The continuous beam model, in which the mass is continuously distributed along the beam length, consists of two continuous beams connected with each other through axially rigid links (Fig. 1a). One of the two continuous beams is a flexural beam, which deforms in a pure flexural type. The other continuous beam is a shear beam, which deforms in a pure shear type. By adjusting the ratio of the shear rigidity of the shear beam to the flexural rigidity of the flexural beam, the continuous beam model is capable of simulating the coupled shear-flexure deformation of tall buildings. The continuous beam model has been broadly applied to the seismic evaluation of tall buildings. To name but a few examples: Kuang and Ng [9] applied the continuous beam model to investigate the characteristics of coupled lateral-torsional free vibration of buildings; Miranda and Taghavi [10] exploited the continuous beam model to estimate the floor accelerations of elastic or essentially elastic buildings subjected to earthquakes; Alimoradi et al. [24] used the continuous beam model for system identification of instrumented buildings; and, based on the theory of uniform continuous shear beams, Wiebe and Christopoulos [25] quantified higher mode effects in multistory buildings.

Inspired by the versatile applications of the continuous beam model (Fig. 1a), Lin [11] proposed the generalized building model (GBM), which consists of one shear stick and one flexural stick (Fig. 1b). The GBM allows irregular distributions of story mass and story stiffness along the building height. In contrast, the continuous beam model (Fig. 1a) simulates buildings with only regular (*e.g.*, uniform, linear, or parabolic) distributions of story mass and story stiffness along the building height. Moreover, because the mass is continuously distributed along the beam length, the continuous beam model is generally only suitable for simulating high-rise buildings. A GBM with discrete (*i.e.*, lumped) masses at floor level is suitable for simulating buildings with any number of stories.

Nevertheless, despite the broadened applicability of the GBM in comparison with the continuous beam model, the existing GBM is only suitable for simulating elastic or essentially elastic buildings. Therefore, the present study aims to extend the existing GBM by incorporating inelastic properties such that this enhanced GBM can serve as a simplified numerical model for estimating the nonlinear seismic response of buildings. The results of this study are expected to provide an alternative method of simplified nonlinear modeling of buildings without restrictions of deformation type, number of stories, and distribution of story mass and/or story stiffness along building heights.

2. Generalized building model

To maintain the integrity of the present paper and avoid duplication, the elastic properties of the GBM are briefly introduced below, and the reader is referred to the relevant literature for more details about its derivations [11,26].

2.1. Elastic properties of the GBM

The GBM (Fig. 1b) simulates an N-story building in which the story diaphragms are rigid and the story heights are h_r, where $r = 1$ to N. The subscript r indicates the story number. The deformation types of the two sticks subjected to lateral loads are pure shear and pure flexure (Fig. 1c

and 1d). These two sticks are laterally connected by axially rigid bars at all story levels. Once the story masses of the N-story building are given, the mass matrix of the GBM is obtained straightforwardly in the form of an $N \times N$ diagonal matrix. The displacement vector of the GBM is expressed as $\mathbf{u} = [u_N \quad u_{N-1} \quad \cdots \quad u_1]^T$, where the subscript of u indicates the story number. The lateral stiffness matrix of the pure shear stick is:

$$\mathbf{K}_s = k_{s,1}\mathbf{E}_s \tag{1}$$

where $k_{s,1} = EI_{s,1}/h_1^3$ and $EI_{s,1}$ is the flexural rigidity of the first story of the pure shear stick (Fig. 1c). The matrix $\mathbf{E_s}$ (Eq. (1)) is defined as:

$$\mathbf{E}_s = 12\begin{bmatrix} \kappa_N & -\kappa_N & 0 & \cdots & 0 & 0 & 0 \\ -\kappa_N & \kappa_N+\kappa_{N-1} & -\kappa_{N-1} & \cdots & 0 & 0 & 0 \\ 0 & -\kappa_{N-1} & \kappa_{N-1}+\kappa_{N-2} & \cdots & 0 & 0 & 0 \\ \vdots & \vdots & \vdots & \ddots & \vdots & \vdots & \vdots \\ 0 & 0 & 0 & \cdots & \kappa_4+\kappa_3 & -\kappa_3 & 0 \\ 0 & 0 & 0 & \cdots & -\kappa_3 & \kappa_3+\kappa_2 & -\kappa_2 \\ 0 & 0 & 0 & \cdots & 0 & -\kappa_2 & \kappa_2+\kappa_1 \end{bmatrix}_{N\times N} \tag{2}$$

In Eq. (2), κ_r ($r = 1$ to N) is the ratio of the lateral stiffness of the rth story to that of the first story. In addition, the lateral stiffness of the rth story can be obtained from elastically pushing the rth story to one unit displacement while the lower stories (*i.e.*, the 1st to the $(r-1)$th stories) remain fixed. The lateral stiffness matrix of the pure flexural stick is defined as:

$$\mathbf{K}_b = \mathbf{F}_b^{-1} \tag{3}$$

where $\mathbf{F}_b$ represents the $N \times N$ flexibility matrix of the pure flexural stick. Using the unit-load method, the ith row and jth column element of $\mathbf{F}_b$, denoted as f_{ij}, is defined as:

$$f_{ij} = \frac{e_{ij}}{k_{b,1}} \tag{4}$$

where $k_{b,1} = EI_{b,1}/h_1^3$ and $EI_{b,1}$ is the flexural rigidity of the first story of the pure flexural stick (Fig. 1d). Parameter e_{ij} (Eq. (4)) is defined as:

$$e_{ij} = \begin{cases} \sum_{r=1}^{N+1-i} \frac{1}{\kappa_r}\left\{ \overline{H}'_{N+1-j}\overline{H}'_{N+1-i}\left(\overline{H}'_r - \overline{H}'_{r-1}\right) - \frac{\left(\overline{H}'^{r}_{N+1-j} + \overline{H}'^{r}_{N+1-i}\right)}{2}\left[\left(\overline{H}'_r\right)^2 - \left(\overline{H}'_{r-1}\right)^2\right] + \frac{1}{3}\left[\left(\overline{H}'_r\right)^3 - \left(\overline{H}'_{r-1}\right)^3\right] \right\}, & i \geqslant j \\ e_{ji}, \quad i < j \end{cases} \tag{5}$$

where $\overline{H}'_s = H_s/h_r$, H_s represents the height measured from the ground to the sth story and h_r is the height of the rth story (Fig. 1d). Therefore, $\mathbf{K}_b$ (Eq. (3)) can be expressed as:

$$\mathbf{K}_b = k_{b,1}\mathbf{E}_b \tag{6}$$

where $\mathbf{E}_b$ is the inverse of the matrix consisting of elements e_{ij}, in which i and j range from 1 to N. The total lateral stiffness matrix of the GBM, denoted as $\mathbf{K}$, is defined as:

$$\mathbf{K} = \mathbf{K}_s + \mathbf{K}_b = k_{s,1}\mathbf{E}_s + k_{b,1}\mathbf{E}_b = k_1[\alpha\mathbf{E}_s + (1-\alpha)\mathbf{E}_b] \tag{7}$$

where:

$$k_1 = k_{s,1} + k_{b,1} = \frac{E\left(I_{s,1} + I_{b,1}\right)}{h_1^3} = \frac{EI_{GBM}}{h_1^3}, \quad \alpha = \frac{k_{s,1}}{k_{s,1} + k_{b,1}} \tag{8}$$

The value of α is between 0 and 1 (Eq. (8)). When α equals zero (*i.e.*, $k_{s,1} = 0$), the deformation type of the GBM is pure flexure (*i.e.*, $\mathbf{K} = k_{b,1}\mathbf{E}_b$). When α equals one (*i.e.*, $k_{b,1} = 0$), the deformation type of the GBM is pure shear (*i.e.*, $\mathbf{K} = k_{s,1}\mathbf{E}_s$). Consequently, the equation of motion of an N-story GBM excluding the velocity term can be expressed as follows:

$$\mathbf{M}\ddot{\mathbf{u}} + \frac{k_1}{m_1}[\alpha\mathbf{E}_s + (1-\alpha)\mathbf{E}_b]\mathbf{u} = -\mathbf{M}\boldsymbol{\iota}\ddot{u}_g \tag{9a}$$

where $\mathbf{M}$ is the mass matrix given as:

$$\mathbf{M} = \begin{bmatrix} \mu_N & & & \mathbf{0} \\ & \ddots & & \\ & & \mu_r & \\ \mathbf{0} & & & \ddots \\ & & & & \mu_1 \end{bmatrix}_{N\times N} \tag{9b}$$

and μ_r is the ratio of the rth story mass (denoted as m_r) to the first story mass (denoted as m_1), $\boldsymbol{\iota}$ is the influence vector, and $\mathbf{0}$ represents the lower and upper triangle zero matrices. $\mathbf{M}$ and $[\alpha\mathbf{E_s} + (1 - \alpha)\,\mathbf{E}_b]$ in Eq. 9 are dimensionless. By varying the value of α from 0 to 1 by a certain increment (*e.g.*, 0.01), a set of GBMs is created. The first three mode shapes of each GBM in that set are computed (Eq. (9a)) and compared with those obtained from the FEM. From those GBMs, the value of α whose corresponding mode shapes best agree with those obtained from the FEM is adopted. The index of the degree of agreement between the mode shapes is the summation of the weighted root mean square of the discrepancy between the first three normalized mode shapes of the GBM and the FEM. In addition, the effective modal participation mass ratio is used as the weighting factor. The value of k_1/m_1 is then determined so that the first vibration period of the GBM with the selected value of α is equal to that of the FEM.

When using a structural analysis program to construct an elastic GBM, the section properties (*e.g.*, sectional moment of inertia) and material properties (*e.g.*, Young's modulus) are required. Equation (8) indicates that the first story stiffness ($k_1 = k_{s,1} + k_{b,1}$) is distributed between the pure shear stick ($k_{s,1}$) and the pure flexural stick ($k_{b,1}$) according to the value of α (*i.e.*, $k_{s,1} = \alpha k_1$, $k_{b,1} = (1-\alpha)\,k_1$). Furthermore, the GBM retains the vital advantage of a continuous beam model that uses a single parameter (α) to effectively characterize the overall deformation type of an N-story building rather than using N parameters (*e.g.*, α_r, $r = 1$ to N) to characterize the deformation types of N stories. Therefore, the rth story stiffness, where $r = 1$ to N, is also distributed between the pure shear stick (denoted as $k_{s,r}$) and the pure flexural stick (denoted as $k_{b,r}$) according to the value of α. It is clear that the rth story stiffness is affected by Young's modulus, the sectional moment of inertia, and the story height (*e.g.*, $k_{s,1} = EI_{s,1}/h_1^3$ and $k_{b,1} = EI_{b,1}/h_1^3$). Therefore, the relative values of the sectional moment of inertia of the rth story of the pure shear stick and the pure flexural stick (denoted respectively as $I_{s,r}$ and $I_{b,r}$) are assigned as $h_r{}^3k_{s,r}$ and $h_r{}^3k_{b,r}$, respectively. The value of Young's modulus (denoted as E) is then selected so that the first vibration period of the GBM is equal to that of the FEM.

2.2. Inelastic properties of the GBM

The two sticks of each story of the GBM are simulated as beam-column elements that have lumped plasticity at their top and bottom. Such an element type is straightforward for the engineering design and analyses of building structures. The collective force–deformation relationship of the two sticks of the rth story of the GBM is expected to reflect

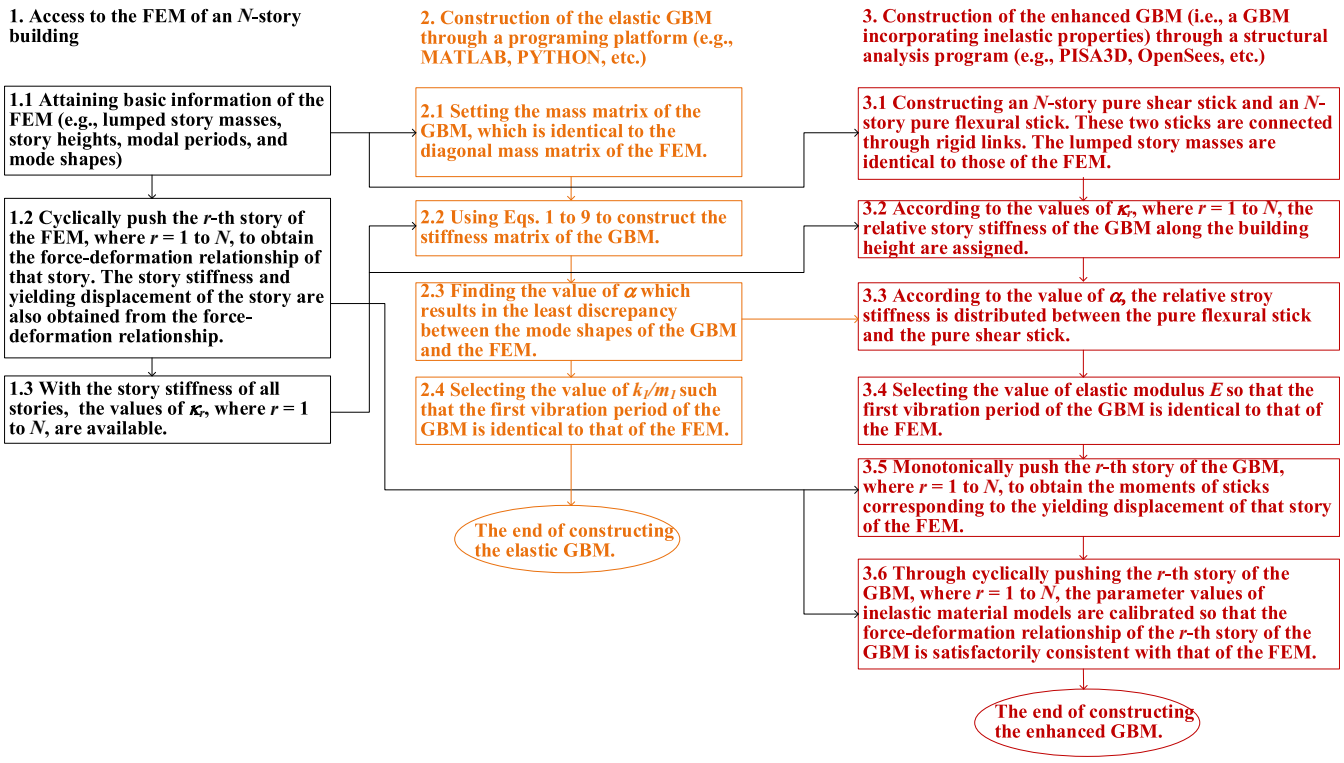

Fig. 2. The framework of constructing an enhanced GBM.

the force–deformation relationship of the rth story of the FEM. The inelastic properties of the two sticks of the GBM are obtained from the following procedure:

Step 1: If a leaning column exists in the FEM of an N-story building for considering P-Δ effect, a leaning column connected with the GBM through rigid links should be constructed. The gravity load of each story is put on top of the corresponding story of the leaning column. Otherwise, this step is skipped.

Step 2: Set $r = 1$, where r indicates the story number.

Step 3: The rth story of the FEM is cyclically pushed while the lower stories are fixed. The force–deformation relationship and the yielding displacement (Δ_{yr}) of the rth story are accordingly obtained.

Step 4: The rth story of the elastic GBM is monotonically pushed while the lower stories are fixed. The moments at the top and bottom of the two sticks of the rth story corresponding to the displacement Δ_{yr} are assigned as their respective yielding moments.

Step 5: The rth story of the GBM is cyclically pushed while the lower stories are fixed. The parameter values of the nonlinear material used for the two sticks of the rth story are accordingly calibrated until the force–deformation relationship of the rth story of the GBM is satisfactorily consistent with that of the FEM obtained from Step 3.

Step 6: If $r < N$, set $r = r + 1$ and go to Step 3. Otherwise, the iteration is stopped. In other words, Steps 3 to 5 are conducted once for each story.

The framework for constructing an enhanced GBM is illustrated in Fig. 2. Once the enhanced GBM has been constructed, the seismic response of the N-story building can be rapidly estimated by conducting NRHA to the GBM instead of to the FEM. From Steps 3 and 4, it is clear that the yielding displacement (Δ_{yr}) is used as an intermediate parameter to determine the yielding moments of the sticks, which are essential for inelastic structural analyses. Engineering demand parameters, which depend on input ground motions, seem to be unsuitable for use as the parameters for construction of the simplified numerical model. It is worth noting that the nonlinear modeling dealt with in this study focuses on the inelastic behavior resulting from the yielding of structural materials. Other factors causing nonlinear structural responses (*e.g.*, large deformations, friction, nonlinear boundary conditions) are outside the scope of the present study.

3. Numerical Validation

The effectiveness of the proposed simplified nonlinear model for estimating the seismic response of buildings was verified using two example buildings: a three-story reinforced concrete (RC) building [26,27] and a nine-story steel building [26]. Because the GBM (Fig. 1b) does not consider the soil-structure interaction, the two example buildings have fixed column bases without soil springs. These numerical validations are described below.

3.1. Three-story RC building

The three-story RC building was tested using the shaking table of Taiwan's National Center for Research on Earthquake Engineering in 2017 [27]. The design drawing of that building specimen is illustrated in Fig. A1 of Appendix A. Because of the elevated first story and the fact that the RC walls were only added to the two exterior sides of the 3rd story (Fig. A1), the building specimen was vertically irregular. The resultant weight of the three-story building was 505 kN in total, and 183.8 kN, 168.9 kN, and 152.3 kN for the first, second, and third stories, respectively. The ground motion of the 1999 Chi-Chi earthquake recorded at station TCU052, which was a near-fault pulse-like motion, was replicated during the shaking table test. The horizontal and vertical components of TCU052 were scaled and applied in the x-direction and z-direction of the building specimen, respectively. The two components were amplified using the same scaling factor. Fig. A2a and A2b display the measured acceleration records of the horizontal and vertical components, respectively. Fig. A2c shows the 5%-damped pseudo-acceleration spectra of the measured acceleration records. The details of the shaking table test and the numerical simulation (FEM) are available in Lin et al. [27]. Using the verified FEM, the first modal vibration period (T_1) was determined to be 0.395 s and the corresponding participation mass ratio was up to 98.63 %. The FEM adopted Rayleigh

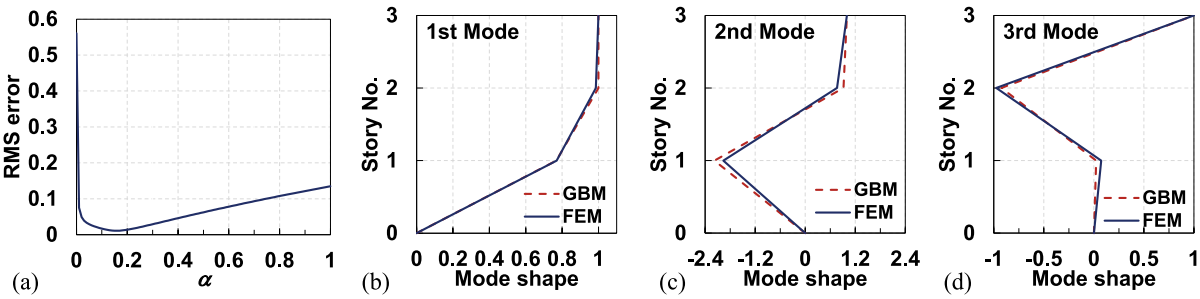

Fig. 3. (a) RMS error as α varies from 0 to 1; (b) the 1st, (c) 2nd, and (d) 3rd mode shapes of the three-story building.

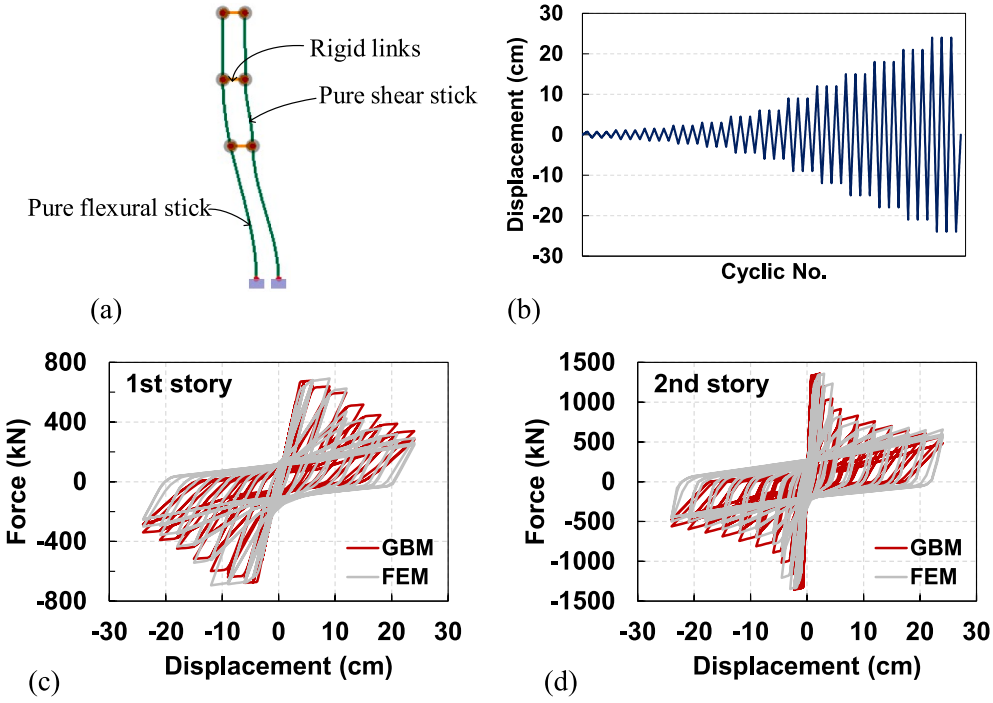

Fig. 4. (a) The 1st mode shape of the GBM; (b) cyclic displacement history; (c) and (d) force–deformation relationships of the 1st and 2nd stories of the FEM compared with those obtained from the GBM.

damping with the damping ratios of the first two x-directional modes equal to 3% to represent the inherent damping of the building. The present study constructed a GBM for estimating the seismic response of the three-story building under the excitation of TCU052.

With $T_1 = 0.395$ s and 3% Rayleigh damping, the remaining elastic properties of the GBM to be determined are α and κ_r, where $r = 1$ to 3. α is a parameter that characterizes the overall deformation type of a multi-story building. κ_r represents the ratio of the lateral stiffness of the rth story to that of the first story. By pushing the rth story (where $r = 1$ to 3) of the FEM of the three-story building while the lower stories are fixed, the elastic story stiffness of the 1st, 2nd, and 3rd stories were obtained as 169.65 kN/cm, 1051.48 kN/cm, and 175,126 kN/cm, respectively. Consequently, κ_1, κ_2, and κ_3 (*i.e.*, the ratios between story stiffnesses) were found to be equal to 1.0, 6.2, and 1032.3, respectively. In addition, by varying α from 0 to 1 with an increment of 0.01, 101 GBMs with the specified values of κ_1, κ_2, and κ_3 were constructed. Among the 101 GBMs, the value of α resulting in the least root-mean-square (RMS) error between the mode shapes obtained from the GBM and FEM was regarded as the optimal value of α. Because the dynamic response of the three-story building was overwhelmingly dominated by the first mode, only the first mode shape was considered when searching for the optimal value of α. Fig. 3a illustrates the RMS error for the 101 GBMs. Accordingly, the optimal value of α for this three-story building was found to be equal to 0.16. As a result, $k_{b,1} = (1-\alpha)/\alpha \times k_{s,1} = 5.25k_{s,1}$ (Eq. (8)). By selecting the relative values of $k_{s,1}$, $k_{s,2}$, and $k_{s,3}$ equal to 1.0, 6.2, and 1032.3 (*i.e.*, κ_1, κ_2, and κ_3), respectively, the relative values of $k_{b,1}$, $k_{b,2}$, $k_{b,3}$ are 5.25 times $k_{s,1}$, $k_{s,2}$, and $k_{s,3}$, respectively. That is to say, the relative values of $k_{b,1}$, $k_{b,2}$, $k_{b,3}$ are 5.25, 32.54, and 5419.4, respectively. It is clear that the values of Young's modulus (denoted as E), the sectional moment of inertia (denoted as $I_{s,r}$, $I_{b,r}$), and story height (denoted as h_r) collectively affect the values of $k_{s,r}$ and $k_{b,r}$ (where $r = 1$ to 3) (*e.g.*, $k_{b,1} = EI_{b,1}/h_1^3$). Because the value of h_r was set equal to the rth story height, the values of $I_{s,r}$ and $I_{b,r}$ were computed as $h_r^3 k_{s,r}$ and $h_r^3 k_{b,r}$, respectively. Moreover, the value of E was selected so that the first vibration period of the GBM was equal to that of the FEM. Fig. 3b-d display the 1st to 3rd mode shapes obtained from the GBM, respectively, compared with those obtained from the FEM. The vibration periods of the first three modes obtained from the GBM were 0.396 s, 0.06 s, and 0.01 s, respectively, which are close to those obtained from the FEM (0.395 s, 0.07 s, and 0.02 s).

This study used the PISA3D structural analysis program [28,29] to construct a numerical model of the GBM. (PISA3D is software developed through the joint effort of Taiwan National Center for Research on Earthquake Engineering and National Taiwan University. PISA3D software can be downloaded for free trial and academic applications with a limited number of nodes (up to 200) at https://www.ncree.org/PISA3D.

Table 1
Yielding displacement and yielding moments at the top and bottom of the sticks of the 1st and 2nd stories of the GBM of the three-story building.

Story No.	1st		2nd	
Δ_y (cm)	3.81		1.26	
Stick type	flexural	shear	flexural	shear
M_{yb} (kN-cm)	96,250	26,870	83,990	16,146
M_{yt} (kN-cm)	51,450	26,870	83,217	16,146

aspx.) Fig. 4a shows a snapshot of the 1st mode shape of the GBM displayed via the graphical user interface (GUI) of PISA3D. Fig. 4a clearly shows the different deformation types of the pure shear stick and the pure flexural stick. The cyclic displacement histories shown in Fig. 4b were separately imposed on each of the 1st and the 2nd stories of the FEM of the three-story building. The induced force–deformation relationships are illustrated as gray lines in Fig. 4c and 4d. It should be noted that the RC walls were simulated as elastic panel elements in the FEM because the deformation of the building was expected to concentrate on the soft 1st story [27]. In other words, the 3rd story was expected to remain elastic. Thus, there was no need of exerting the cyclic displacements on the 3rd story.

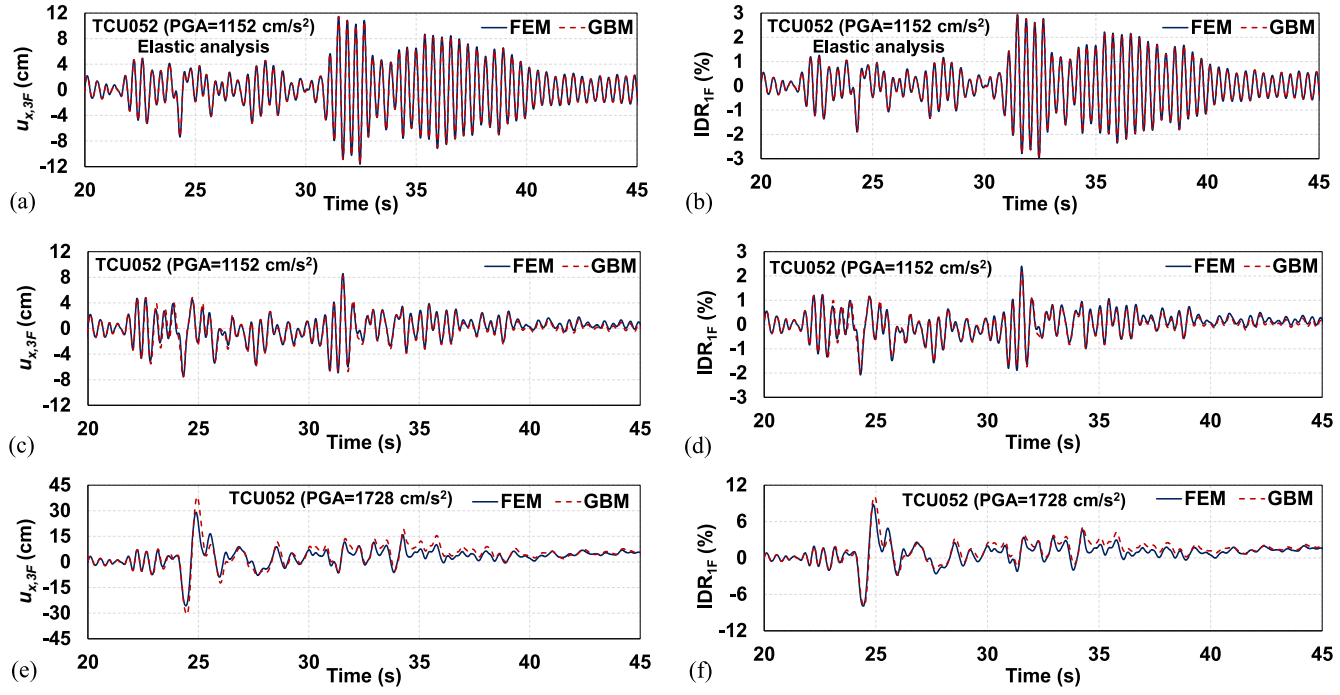

Fig. 5. Elastic response histories of (a) $u_{x,3F}$, and (b) IDR_{1F} of the three-story building subjected to TCU052 ground motion scaled to a PGA of 1152 cm/s^2; nonlinear response histories of (c) $u_{x,3F}$, and (d) IDR_{1F} of the three-story building under TCU052 scaled to a PGA of 1152 cm/s^2; nonlinear response histories of (e) $u_{x,3F}$, and (f) IDR_{1F} of the three-story building under TCU052 scaled to a PGA of 1728 cm/s^2.

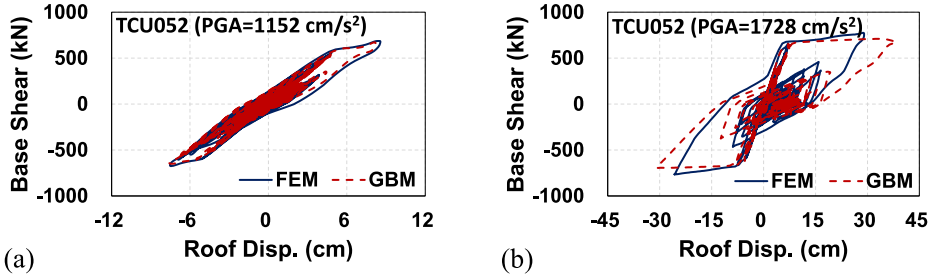

Fig. 6. Hysteretic loops of roof displacement versus base shear of the three-story building under TCU052 ground motion scaled to a PGA of (a) 1152 cm/s^2 and (b) 1728 cm/s^2.

Table 2
Lateral stiffness and κ values of the nine-story building.

rth story	1	2	3	4	5	6	7	8	9
Lateral stiffness (kN/cm)	3685	8668	7740	7629	6183	5960	4247	4075	2851
κ_r	1.00	2.35	2.10	2.07	1.68	1.62	1.15	1.11	0.77
$k_{s,r}$	1.00	2.35	2.10	2.07	1.68	1.62	1.15	1.11	0.77
$k_{b,r}$	3.76	8.85	7.90	7.79	6.31	6.08	4.34	4.16	2.91

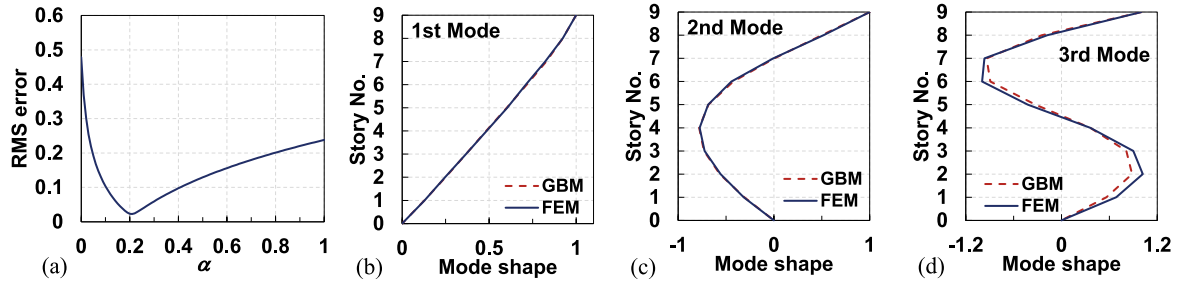

Fig. 7. (a) RMS error as α varies from 0 to 1; (b) 1st, (c) 2nd, and (d) 3rd mode shapes of the nine-story building.

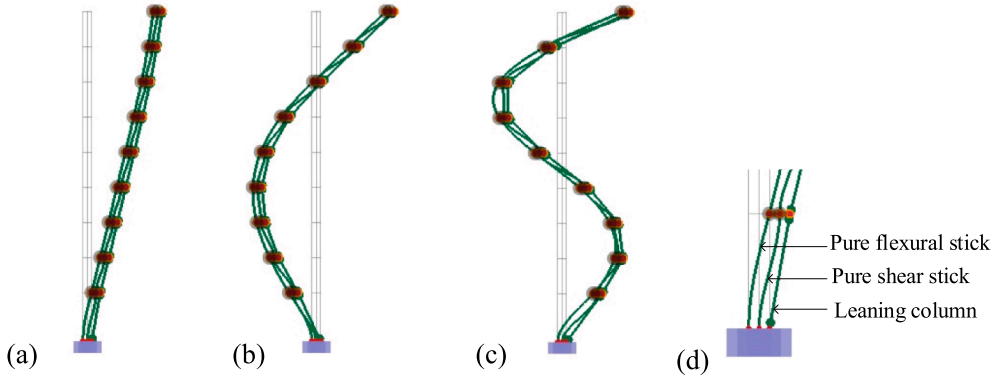

Fig. 8. Snapshots of the (a) 1st, (b) 2nd, and (c) 3rd mode shapes of the GBM displayed via the GUI of PISA3D. (d) Close-up of (a).

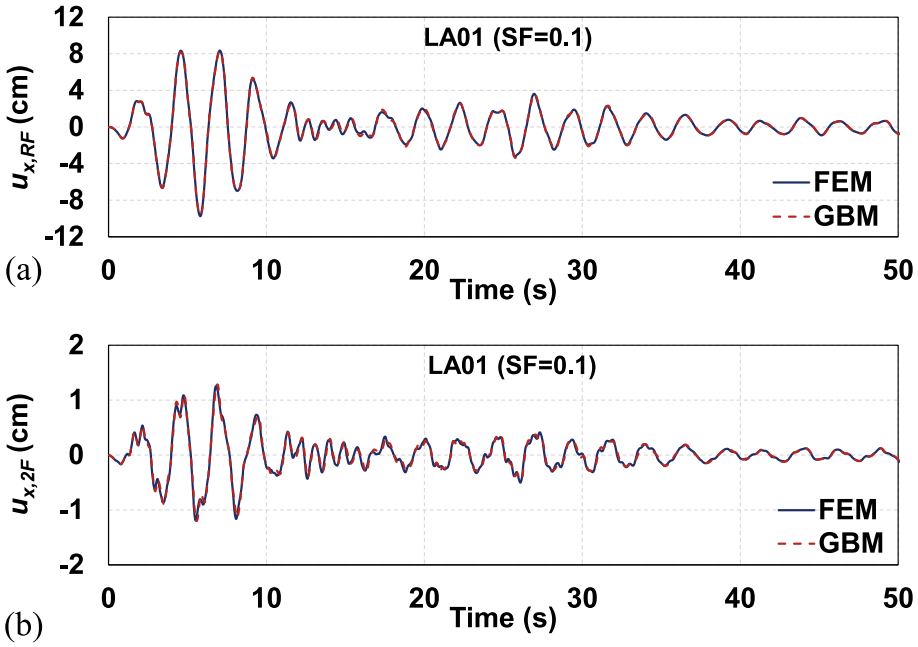

Fig. 9. (a) $u_{x,RF}$, and (b) $u_{x,2F}$ of the GBM and FEM subjected to LA01 multiplied by a scaling factor of 0.1.

Fig. 4c and 4d show that the yielding displacements of the 1st and 2nd stories of the FEM (*i.e.*, Δ_{y1} and Δ_{y2}) were 3.8 cm and 1.26 cm, respectively. By monotonically pushing the elastic GBM, the yielding moments at the top and bottom of the sticks of the 1st and 2nd stories (*i.e.*, the moments corresponding to displacements Δ_{y1} and Δ_{y2}, respectively) were obtained and are listed in Table 1. It is clear that the force–deformation relationships of RC structures exhibit characteristics of pinching phenomena and degradation in stiffness and strength. Therefore, a degrading material available in the PISA3D structural analysis program that characterizes stiffness degradation, strength degradation, and pinching was selected to simulate the RC building. The parameters of the degrading material used for the sticks were calibrated such that the force–deformation relationships of the GBM (illustrated as red lines in Fig. 4c and 4d) were satisfactorily consistent with those obtained from the FEM. This concluded the construction of the nonlinear GBM representing the three-story building.

In order to verify the validity of the elastic GBM, elastic seismic analyses of the GBM and FEM were conducted using the acceleration

Table 3
Yielding displacement (Δ_y) and yielding moments (M_{yt} and M_{yb}) of the two sticks of all stories of the GBM.

Story No.	1st		2nd		3rd	
Δ_y (cm)	5.76		3.36		3.36	
Stick type	flexural	shear	flexural	shear	flexural	shear
M_{yb} (MN-cm)	6070	2170	5750	2160	5220	1930
M_{yt} (MN-cm)	2880	2170	2290	2160	2190	1930
Story No.	**4th**		**5th**		**6th**	
Δ_y (cm)	3.3		3.36		3.36	
Stick type	flexural	shear	flexural	shear	flexural	shear
M_{yb} (MN-cm)	4690	1790	4080	1510	3840	1490
M_{yt} (MN-cm)	1730	1790	1720	1510	1320	1490
Story No.	**7th**		**8th**		**9th**	
Δ_y (cm)	3.75		3.6		4.2	
Stick type	flexural	shear	flexural	shear	flexural	shear
M_{yb} (MN-cm)	3200	1180	2870	1120	1960	921
M_{yt} (MN-cm)	1360	1180	964	1120	NA	921

records of TCU052 in the shaking table tests (Fig. A2a and A2b). The peak ground acceleration (PGA) of the measured x-directional acceleration record was 1152 cm/s^2 (Fig. A2a). Fig. 5a and 5b respectively show the roof displacement histories (denoted as $u_{x,3F}$) and the IDR histories of the 1st story (denoted as IDR$_{1F}$) obtained from the GBM and the FEM. The accuracy of the elastic numerical model of the GBM is confirmed in Fig. 5a and 5b. Fig. 5c and 5d are the counterparts of Fig. 5a and 5b and show the results of the nonlinear seismic analyses of the GBM and FEM. The peak values of $u_{x,3F}$ and IDR$_{1F}$ obtained from the GBM were 8.22 cm and 2.16%, respectively, in comparison with 8.57 cm and 2.40% obtained from the FEM (Fig. 5c and 5d). Furthermore, the measured acceleration records of TCU052 were amplified by a factor of 1.5 (*i.e.*, PGA = 1728 cm/s^2) and then used as the input ground motion. Fig. 5e and 5f respectively show the histories of $u_{x,3F}$ and IDR$_{1F}$ obtained from the GBM and the FEM input with the amplified ground motion. Under such strong shaking, the peak values of $u_{x,3F}$ and IDR$_{1F}$ obtained from the GBM were 39.5 cm and 9.95%, respectively, in comparison with 29.04 cm and 8.82% obtained from the FEM (Fig. 5e and 5f). According to the incremental dynamic analyses (IDA) conducted in a previous study [27], the three-story building collapses when subjected to an amplified TCU052 with a corresponding $S_a(T_1,5\%)$ equal to or greater than 3.25 g, where $S_a(T_1,5\%)$ is the 5%-damped pseudo-acceleration spectrum at the first vibration period. Because the PGA of TCU052 is approximately one half of $S_a(T_1,5\%)$ (Fig. A2c), the building collapses under the exertion of the further amplified TCU052 with a PGA of 1728 cm/s^2 (*i.e.*, $S_a(T_1,5\%) \fallingdotseq 3.4$ g). Fig. 6a and 6b illustrate the hysteretic loops of roof displacement versus base shear under the excitation of the amplified TCU052 with a PGA of 1152 cm/s^2 and 1728 cm/s^2, respectively. Figs. 5 and 6 together indicate that the nonlinear GBM is a satisfactory substitute for the FEM to estimate the full range of seismic responses (from an elastic state to collapse) of the three-story building subjected to TCU052 ground motion.

3.2. Nine-story steel building

A nine-story steel building was the prototype building used in the SAC steel research project for buildings located in Los Angeles [30]. The SAC steel research project is a joint venture of the Structural Engineers Association of California (SEAOC), Applied Technology Council (ATC), and California Universities for Research in Earthquake Engineering (CUREe). Fig. B1 of Appendix B illustrates the floor plan, elevation, and member sizes of the nine-story building, in which the perimeter frame is a moment-resisting frame; the gravity columns encircled by the perimeter frame are not displayed. The materials constituting the beams and columns of the nine-story building are Dual A36 Gr. 50 steel and A572 Gr. 50 steel, respectively. The yield strengths, denoted as F_y, of these two steel materials, are 340 MPa and 345 MPa, respectively. Both steel materials were simulated as bilinear materials with a Young's modulus $E = 2.0 \times 10^5$ MPa and a 2% post-yielding stiffness ratio. The story masses of the top to the bottom stories are 1067, 990.8, 990.8, 990.8, 990.8, 990.8, 990.8, 990.8, and 1008 tons. The ensemble of 20 earthquake records (denoted as LA01 to LA20) employed in the SAC steel research project for the hazard level of a 475-year return period in Los Angeles was applied in the x-direction of the nine-story building in the present study. In addition, Rayleigh damping was assigned to the building model whereby the damping ratios of the first two x-directional modes were set to 2%. Fig. B2 shows the 2%-damped pseudo-acceleration spectra of the ensemble of earthquake records.

By conducting pushover analysis of the rth story (where $r = 1$ to 9) of

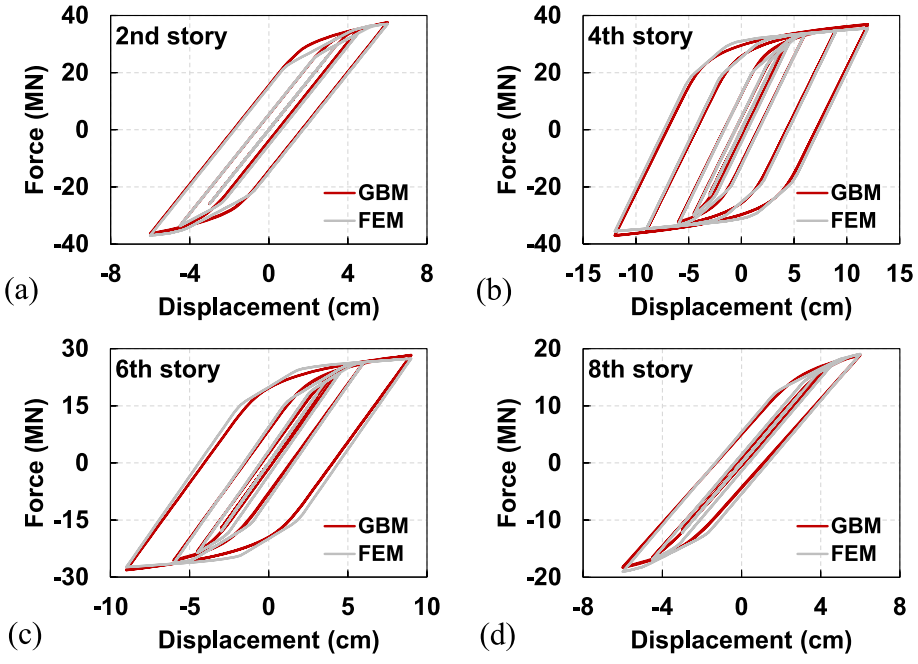

Fig. 10. The force–deformation relationships of the (a) 2nd, (b) 4th, (c) 6th, and (d) 8th stories of the FEM and the GBM.

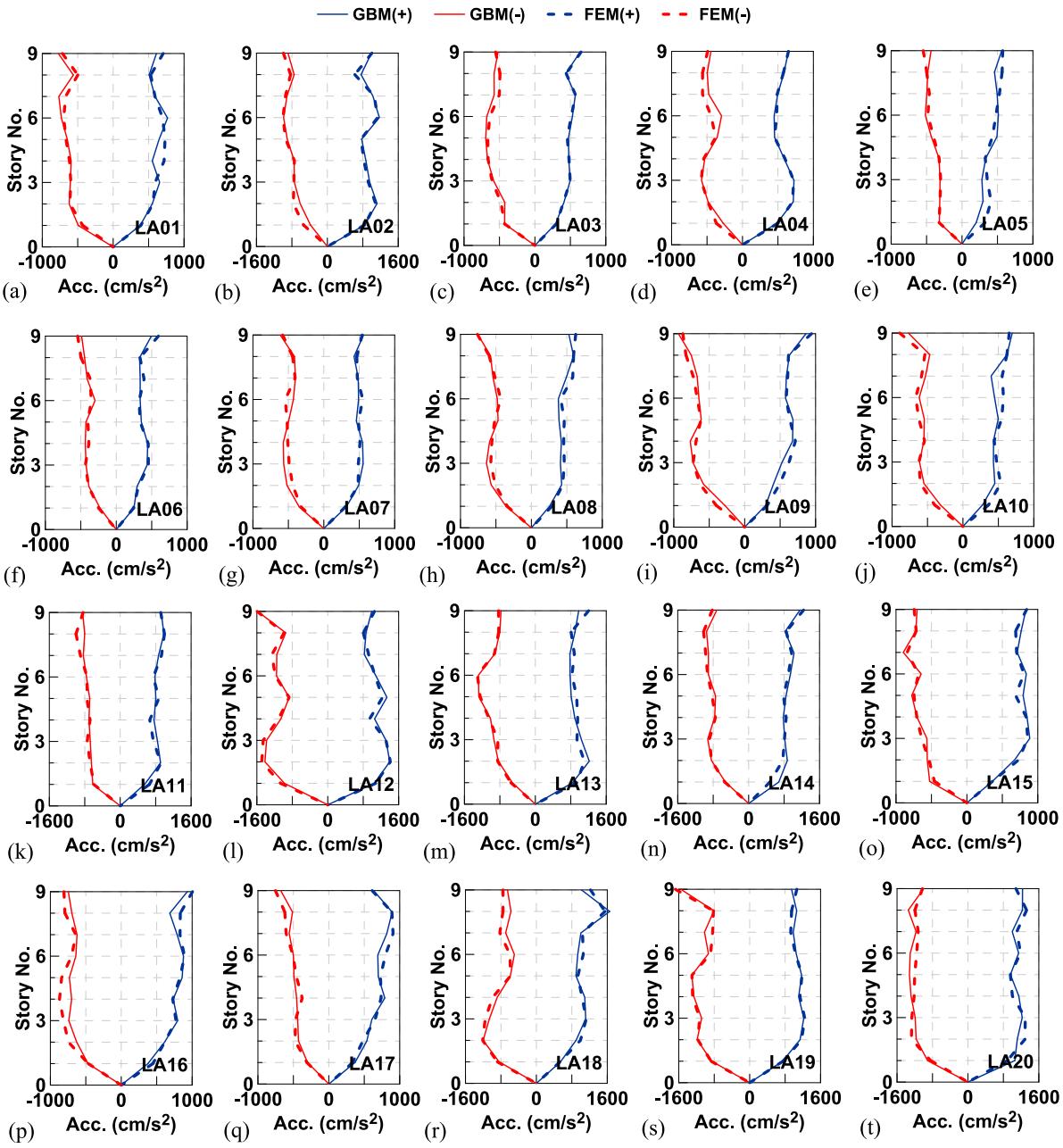

Fig. 11. Peak story accelerations along the building height as the nine-story building was subjected to the indicated ground motions (LA01 to LA20).

the FEM of the nine-story building while the lower stories were fixed, the lateral stiffness and the κ value of each story were obtained (Table 2). Fig. 7a shows the RMS error of the estimated first three mode shapes of the GBMs with the specified κ values (Table 2) when the α value varied from 0 to 1. It is worth noting that the modal participation mass ratios were used as weights when summing the RMS errors of the estimated first three mode shapes. From Fig. 7a, it is evident that the optimal value of α is equal to 0.21. As a result, $k_{b,1} = (1-\alpha)/\alpha \times k_{s,1} = 3.76k_{s,1}$ (Eq. A8). The relative values of $k_{s,r}$, and $k_{b,r}$ ($r = 1$ to 9) are listed in Table 2. It is worth noting that because the story heights are not identical, the sectional moments of inertia, $I_{s,r}$ and $I_{b,r}$, of the sticks of the GBM were adjusted as $h_r{}^3 k_{s,r}$ and $h_r{}^3 k_{b,r}$, respectively. The value of Young's modulus was set so that the first vibration period of the GBM was equal to that of the FEM of the nine-story building. Fig. 7b to 7d illustrate the first three mode shapes obtained from the GBM (α = 0.21) and the FEM. In addition, the vibration periods of the 1st to 3rd modes obtained from the GBM are 2.37 s, 0.89 s, and 0.52 s, respectively, which are close to those obtained from the FEM (*i.e.*, 2.37 s, 0.88 s, and 0.50 s). The modal participation mass ratios of the 1st to 3rd modes obtained from the GBM are 0.807, 0.115, and 0.039, respectively, which are also close to those obtained from the FEM (*i.e.*, 0.807, 0.114, and 0.043). Fig. 8a to 8c are snapshots of the mode shapes of the first three modes of the GBM displayed via the GUI of PISA3D. Fig. 8d, a close-up of Fig. 8a, clearly shows the different deformation types of the pure shear stick and the pure flexural stick. In addition, a leaning column was connected with the GBM in order to consider the P-Δ effect of the gravity columns of the nine-story building.

One of the 20 ground motion records, a record of the 1944 El Centro earthquake (denoted as LA01), was multiplied by a scaling factor (SF) of 0.1 to verify the validity of the elastic GBM constructed using the PISA3D structural analysis program. Fig. 9 shows the displacement histories on the roof and 2nd story of the GBM and FEM, respectively denoted as $u_{x,RF}$ and $u_{x,2F}$. Fig. 9 confirms the validity of the elastic GBM. It is interesting to note that the higher-mode effect appears to be greater

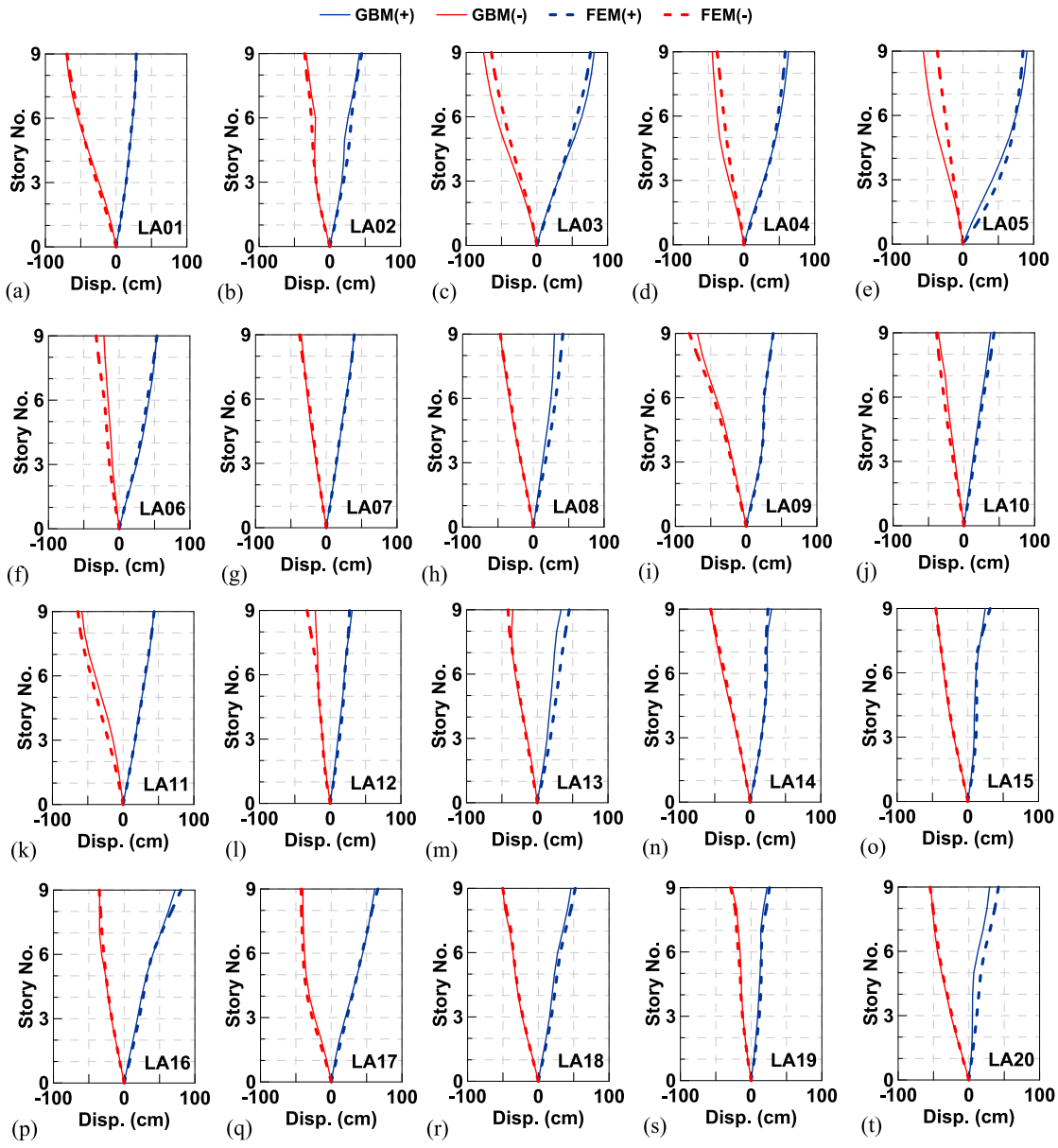

Fig. 12. Peak story displacements along the building height as the nine-story building was subjected to the indicated ground motions (LA01 to LA20).

in the displacement response of the 2nd story than the roof (Fig. 9).

In order to determine the inelastic properties of the GBM, each story of the FEM was cyclically pushed while the lower stories were fixed. The yielding displacement (denoted as Δ_y) of each story was thus obtained from the force–deformation relationship of the corresponding story of the FEM. Moreover, by monotonically pushing the elastic GBM while the lower stories were fixed, the moments of the two sticks of each story of the GBM corresponding to the yielding displacement (Δ_y) were assigned as the yielding moments (denoted as M_{yt} and M_{yb}). M_{yt} and M_{yb} represent the yielding moments at the top and bottom of the sticks, respectively. Table 3 lists the yielding displacements and yielding moments of the two sticks of all stories of the GBM.

Because the force–deformation relationships of steel structures are generally stable, a hardening material using the two-surface plastic hardening rule was selected for the sticks of the GBM. The associated parameter values that control isotropic hardening and kinematic hardening in PISA3D were determined by calibrating the force–deformation relationships obtained by cyclically pushing the GBM to be as alike as possible to those obtained from the FEM. Fig. 10 shows the ultimate force–deformation relationships of the 2nd, 4th, 6th, and 8th stories of the GBM compared with those obtained from the FEM. This concludes the construction of the nonlinear GBM representing the nine-story building.

NRHA of the GBM and FEM of the nine-story building was conducted for the ensemble of 20 ground motion records (LA01 to LA20). Figs. 11, 12, and 13 respectively show the peak story accelerations, the peak story displacements, and the peak inter-story drift ratios (IDRs) along the height of the building under the excitation of the 20 ground motions. Figs. 11-13 collectively indicate that the GBM satisfactorily estimated both the values and distributions of the peak responses along the building height of the nine-story building subjected to the ground motions with the seismic hazard of a 475-year return period. In general, the estimates of the peak IDRs (Fig. 13) are not as accurate as those of the peak floor accelerations (Fig. 11) and the peak floor displacements (Fig. 12). It is clear that IDRs are obtained from the differences between story displacement histories. As a result, the accuracy of the peak IDR estimates are affected not only by the magnitude but also by the happening time of the floor displacement estimates. Fig. 14a and 14b compare the peak IDRs of all stories and the normalized peak base shear (denoted as V/W) estimated using the GBM with those obtained from the

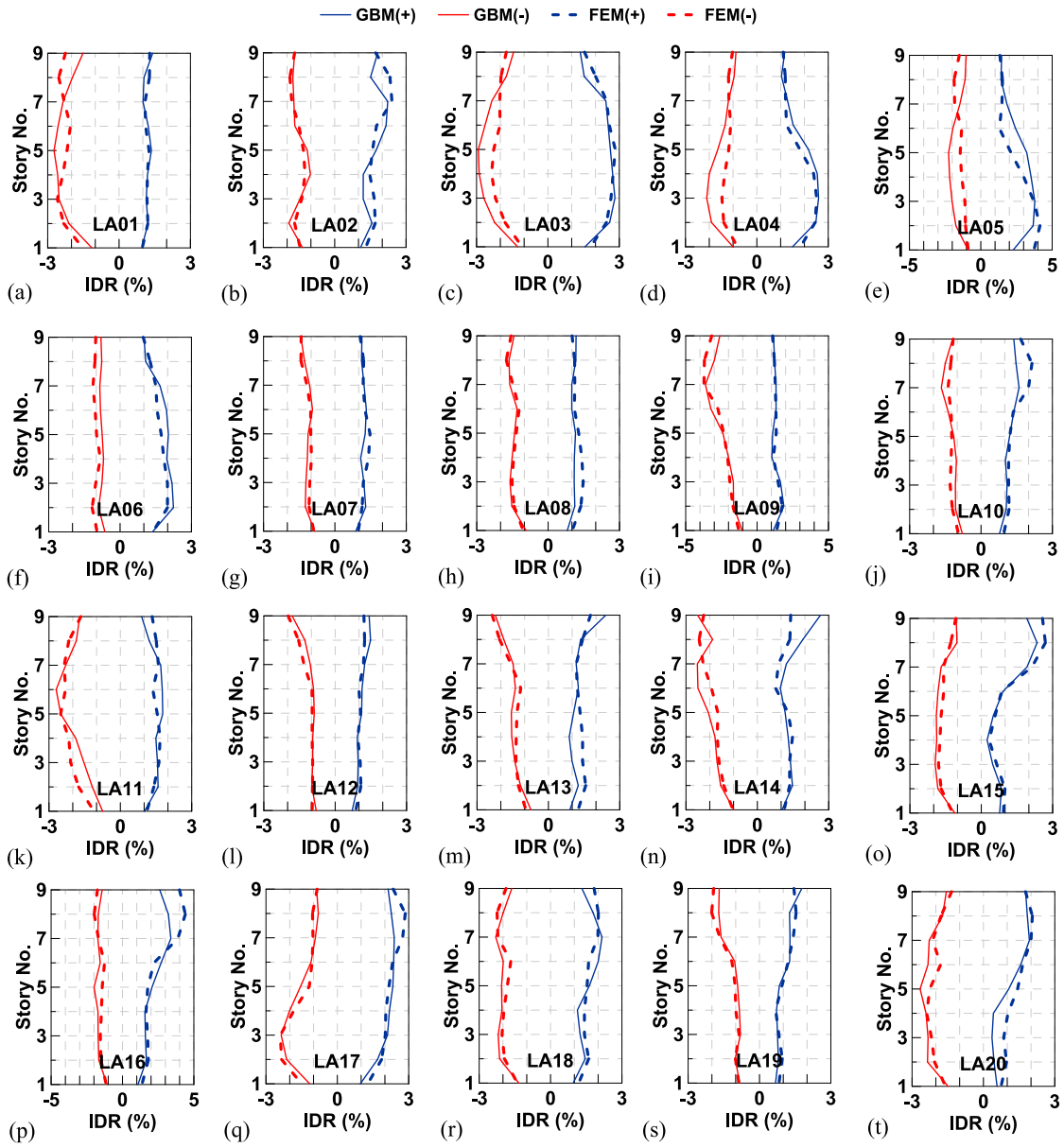

Fig. 13. Peak inter-story drift ratios along the building height as the nine-story building was subjected to the indicated ground motions (LA01 to LA20).

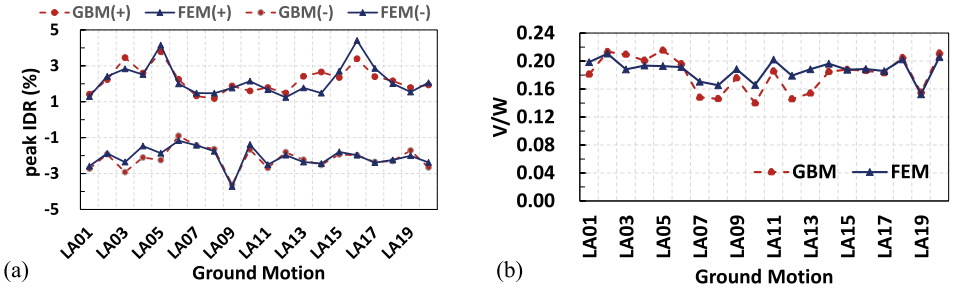

Fig. 14. (a) Positive and negative peak IDR and (b) normalized peak base shears of the nine-story building subjected to the 20 ground motions.

FEM, respectively. V and W denote the peak base shear and building weight (88394 kN), respectively. Fig. 14 clearly indicates that the nine-story building experienced an excursion beyond 2% IDR and sustained a base shear beyond 0.18 times the building weight for most of the 20 ground motion records.

Taking LA01 as an example, the acceleration and displacement histories of the 9th floor (*i.e.*, the roof) and the history of the base shear were examined and are shown in Fig. 15a to 15c. The hysteretic loop of roof displacement versus base shear is illustrated in Fig. 15d. In addition, the history of the IDR of every story of the building is displayed in Fig. 16. Fig. 15b clearly reflects the accuracy of the peak floor displacement estimate of the 9th story shown in Fig. 12a. Moreover,

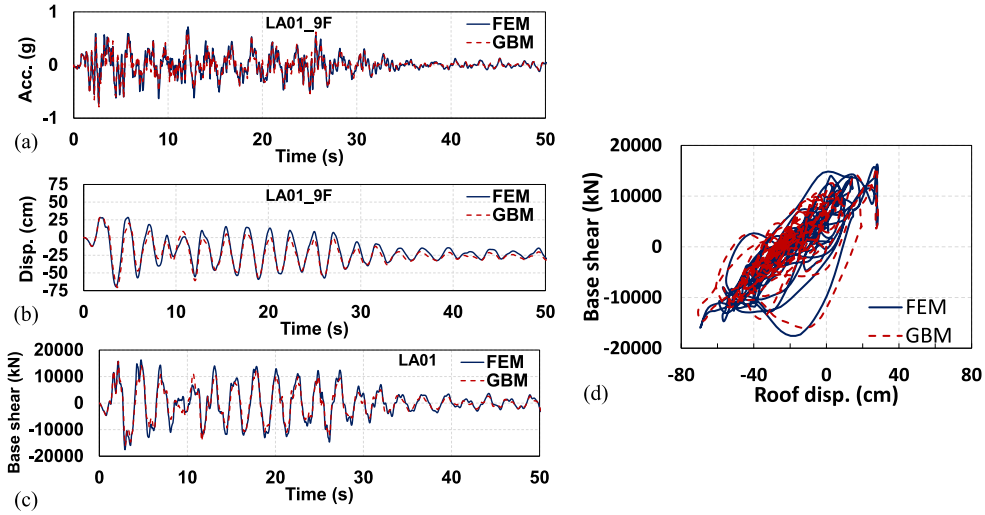

Fig. 15. Histories of (a) roof (9F) acceleration, (b) roof (9F) displacement, (c) base shear, and (d) hysteretic loop of roof displacement versus base shear in response to ground motion LA01.

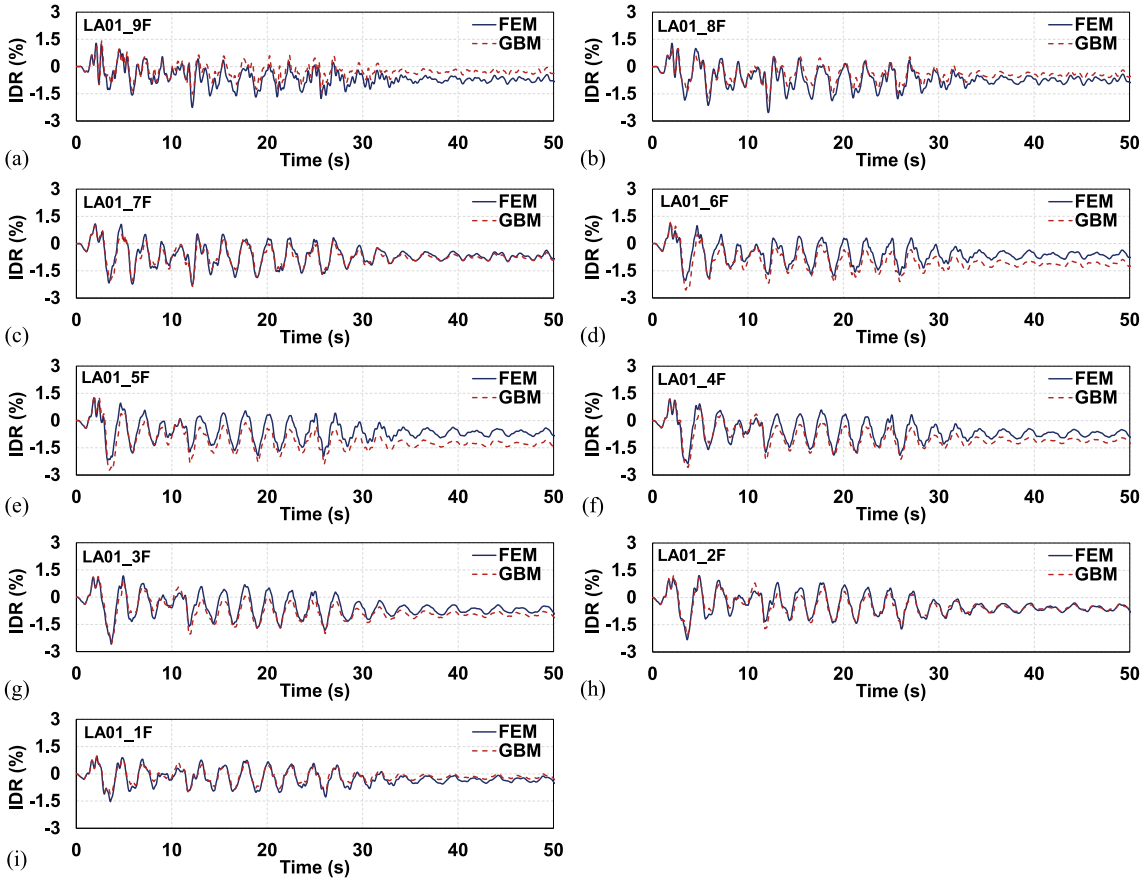

Fig. 16. Histories of IDR of (a)-(i) the 9th floor to the 1st floor of the nine-story building in response to ground motion LA01.

Fig. 16a and 16e respectively reflect the underestimated peak IDR of the 9th story and the overestimated peak IDR of the 5th story illustrated in Fig. 13a. These comparisons may be helpful for understanding why the differences between the peak IDR values obtained from the GBM and the FEM are significant for certain ground motion records (Fig. 13) but the corresponding peak floor displacement estimates are satisfactorily accurate (Fig. 12). Figs. 15 and 16 together indicate that the GBM effectively estimated not only the peak values but also the phases of the seismic responses of the nine-story building in response to LA01. In general, the GBM is a viable alternative simplified nonlinear model for estimating the seismic response of the nine-story building. In addition to the three-story vertically irregular infilled RC building and the nine-story steel moment resisting frame building, other buildings with various structural systems, and vibration periods are worthy of future examination.

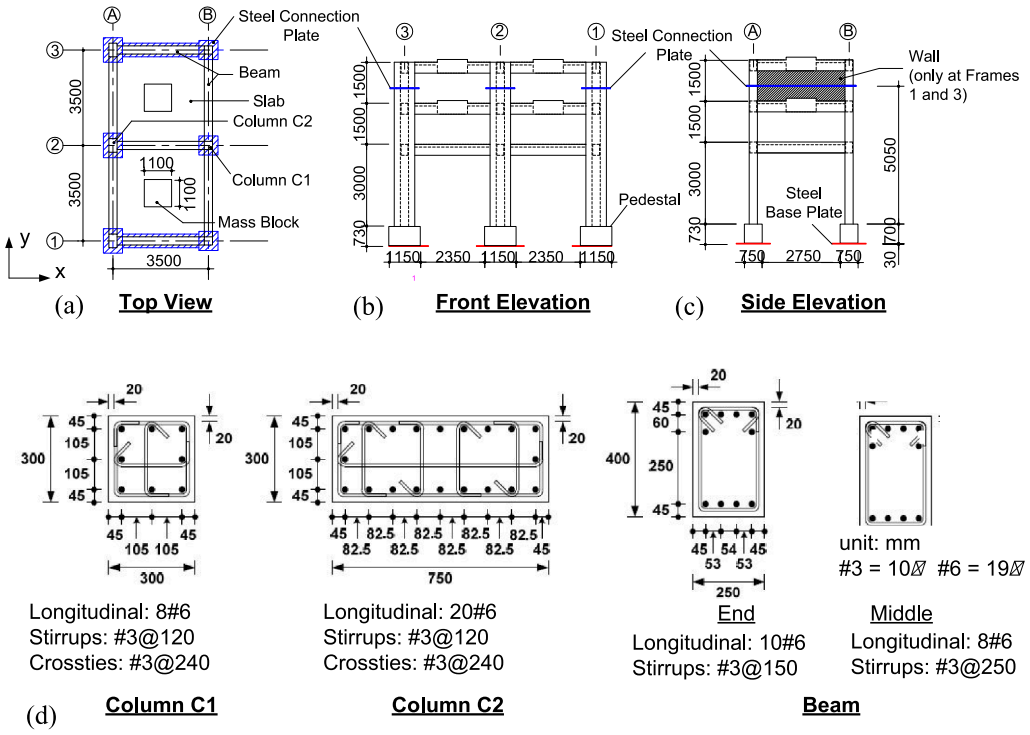

Fig. A1. (a) Top view, (b) front elevation, and (c) side elevation of the three-story building; (d) reinforcement details of the beams and columns.

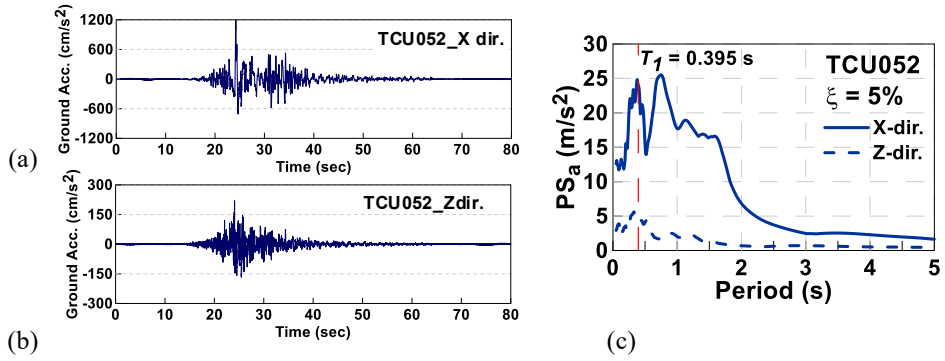

Fig. A2. The measured (a) x-directional and (b) z-directional acceleration records on the shaking table top surface while scaling TCU052 to the PGA = 1000 cm/s^2; (c) 5%-damped pseudo-acceleration spectra of the measured TCU052.

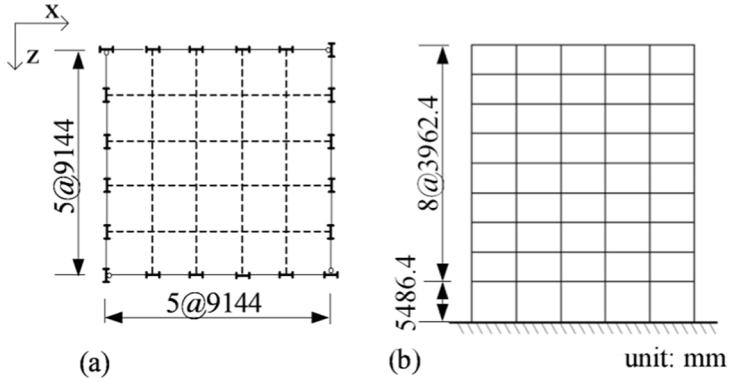

Floor	Columns		Girder
	at corners	elsewhere	
1	W14×370	W14×500	W36×150
2	W14×370	W14×500	W36×150
3	W14×370	W14×455	W33×141
4	W14×370	W14×455	W33×141
5	W14×283	W14×370	W33×141
6	W14×283	W14×370	W33×130
7	W14×257	W14×283	W27×102
8	W14×257	W14×283	W27×94
9	W14×233	W14×257	W24×62

Fig. B1. (a) Typical floor plan, (b) elevation, and (c) member sizes of the nine-story building.

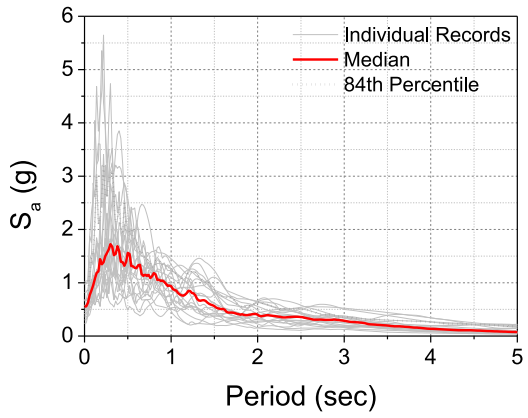

Fig. B2. 2%-damped pseudo-acceleration spectra of the ensemble of 20 earthquake records as well as their median and 84th percentile.

4. Summary and conclusions

This study developed a methodology that incorporated inelastic properties into the original elastic generalized building model (GBM). The effectiveness of the enhanced GBM (*i.e.*, the GBM with inelastic properties) was satisfactorily verified by estimating the seismic responses of a three-story vertically irregular reinforced concrete (RC) building and a nine-story steel moment resisting frame building. The enhanced GBM satisfactorily estimated the full range of seismic responses of the RC building (from an elastic state to collapse) subjected to the TCU052 ground motion record of the 1999 Chi-Chi earthquake. In addition, the enhanced GBM effectively estimated the seismic responses of the steel building subjected to an ensemble of 20 ground motion records with a hazard level of a 475-year return period.

The inelastic properties of the *r*th story of the GBM were determined from the force–deformation relationship of the *r*th story of the finite element model (FEM), which was acquired by imposing cyclic displacements on the *r*th story while the lower stories were fixed. Because the force–deformation relationships of the RC building were characterized by strength degradation, stiffness degradation, and pinching, a degrading material was selected to represent the inelastic properties of the corresponding GBM. Because the force–deformation relationships of the steel building were stable, a hardening material was also selected to represent the inelastic properties of the corresponding GBM. The results indicate that the enhanced GBM is highly versatile and able to simulate buildings with various force–deformation relationships. It is thus expected to be capable of and suitable for the seismic risk assessment of densely urbanized areas.

The enhanced GBM still has limitations. For instance, it does not address the issues of plan asymmetry, supplemental damping, and soil-structure interaction, and these issues and applications are worthy of future exploration.

Declaration of Competing Interest

The authors declare that they have no known competing financial interests or personal relationships that could have appeared to influence the work reported in this paper.

Data availability

Data will be made available on request.

Acknowledgments

The authors gratefully acknowledge the financial support given by the National Science and Technology Council, R.O.C. to this research under Grant No. MOST 110-2625-M-492-004.

Appendix A

References

[1] Fajfar P. Structural analysis in earthquake engineering—a breakthrough of simplified non-linear methods. *12th European Conference on Earthquake Engineering* 2002; paper reference 843.
[2] Chopra AK. Dynamics of structures—theory and applications to earthquake engineering. 3rd edition. NJ, USA: Pearson Prentice Hall; 2007.
[3] Lin JL, Tsai KC. Simplified seismic analysis of asymmetric building systems. Earthq Eng Struct Dyn 2007;36:459–79.
[4] Lin JL, Tsai KC. Seismic analysis of two-way asymmetric building systems under bi-directional seismic ground motions. Earthq Eng Struct Dyn 2008;37:305–28.
[5] Nakashima M, Ogawa K, Inoue K. Generic frame model for simulation of earthquake responses of steel moment frames. Earthq Eng Struct Dyn 2002;31(3):671–92.
[6] Khaloo AR, Khosravi H. Modified fish-bone model: A simplified MDOF model for simulation of seismic responses of moment resisting frames. Soil Dyn Earthq Eng 2013;55:195–210.
[7] Rosman R. Laterally loaded systems consisting of walls and frames. Tall Buildings: Pergamon Press Ltd, London, England; 1967. p. 273–89.
[8] Heidebrecht AC, Smith BS. Approximate analysis of tall wall-frame structures. *J Struct Division*, Proceedings of ASCE 1973;ST2:199–221.
[9] Kuang JS, Ng SC. Coupled vibration of tall building structures. Struct Design Tall Spec Build 2004;13:291–303.
[10] Miranda E, Taghavi S. Approximate floor acceleration demands in multistory buildings I: formulation. *J Struct Eng*, ASCE 2005;131(2):203–11.
[11] Lin JL. Approximate quantification of higher-mode effects on the seismic demands of buildings. Int J Struct Stab Dyn 2019;9(13):1950023.
[12] Inel M, Cayci BT, Meral E. Nonlinear static and dynamic analyses of RC buildings. Int J Civil Eng 2018;16:1241–59.
[13] Aschheim M, Tjhin T, Comartin C, Hamburger R, Inel M. The scaled nonlinear dynamic procedure. Eng Struct 2007;29(7):1422–41.
[14] Oncu ME, Yon MS. Assessment of nonlinear static and incremental dynamic analyses for RC structures. Comput Concr 2016;18(6):1195–211.
[15] Kapos AJ, Penelis GG, Drakopoulos CG. Evaluation of simplified models for lateral load analysis of unreinforced masonry buildings. *J Struct Eng* ASCE 2002;128:1–8.
[16] Lagomarsino S, Penna A, Galasco A, Cattari S. TREMURI program: an equivalent frame model for the nonlinear seismic analysis of masonry buildings. Eng Struct 2013;56:1787–99.
[17] Rodrigues H, Varum H, Costa A. Simplified macro-model for infill masonry panels. J Earthq Eng 2010;14:390–416.
[18] Grange S, Kotronis P, Mazars J. A macro-element to simulate dynamic soil-structure interaction. Eng Struct 2009;31:3034–46.
[19] Jamšek A, Dolšek M. Seismic analysis of older and contemporary reinforced concrete frames with the improved fish-bone model. Eng Struct 2020;212:110514.
[20] d'Aragona MG, Polese M, Prota A. Stick-IT: a simplified model for rapid estimation of IDR and PFA for existing low-rise symmetric infilled RC building typologies. Eng Struct 2020;223:111182.
[21] Ruggieri S, Chatzidaki A, Vamvatsikos D, Uva G. Reduced-order models for the seismic assessment of plan-irregular low-rise frame buildings. Earthq Eng Struct Dyn 2022;51(14):3327–46.
[22] Blasone V, Basaglia A, Risi RD, Luca FD, Spacone E. A simplified model for seismic safety assessment of reinforced concrete buildings: framework and application to a 3-storey plan-irregular moment resisting frame. Eng Struct 2022;250:113348.
[23] Lachanas CG, Vamvatsikos D. Model type effects on the estimated seismic response of a 20-story steel moment resisting frame. *J Struct Eng*, ASCE 2021;147(6).
[24] Alimoradi A, Miranda E, Taghavi S, Naeim F. Evolutionary modal identification utilizing coupled shear-flexural response—implication for multistory buildings Part I: theory. Struct Design Tall Spec Build 2006;15:51–65.
[25] Wiebe L, Christopoulos C. A cantilever beam analogy for quantifying higher mode effects in multistory buildings. Earthq Eng Struct Dyn 2015;44(11):1697–716.
[26] Lin JL, Kek MK, Tsai KC. Stiffness configuration of strongbacks to mitigate inter-story drift concentration in buildings. Eng Struct 2019;199:109615.
[27] Lin JL, Chen WH, Hsiao FP, Weng YT, Shen WC, Weng PW, et al. Simulation and analysis of a vertically irregular building subjected to near-fault ground motions. Earthq Spectra 2020;36(3):1485–516.
[28] Lin BZ, Chuang MC, Tsai KC. Object-oriented development and application of a nonlinear structural analysis framework. Adv Eng Softw 2009;40:66–82.
[29] Tsai KC, Lin BZ. Development of an object-oriented nonlinear static and dynamic 3D structural analysis program, Report no. CEER-92-04. Taipei, Taiwan: Center for Earthquake Engineering Research, National Taiwan University (in Chinese); 2003.
[30] FEMA-355C. State of the art report on systems performance of steel moment frames subject to earthquake ground shaking. prepared by the SAC Joint Venture for the Federal Emergency Management Agency 2000.